

EXPLORATION OF THE SOLAR SYSTEM WITH THE TWO-CHANNEL FOCAL REDUCER AT THE 2m-RCC TELESCOPE OF THE PIK TERSKOL OBSERVATORY

K. Jockers¹, T. Credner¹, T. Bonev², N. Kiselev³, P. Korsun⁴, I. Kulyk⁴, V. Rosenbush⁴, A. Andrienko⁵, N. Karpov⁵, A. Sergeev⁵, and V. Tarady⁵

© 2000

¹*Max-Planck-Institut für Aeronomie
D-37191 Katlenburg-Lindau, Germany
e-mail: jockers@linmpi.mpg.de*

²*Institute of Astronomy of Bulgarian Academy of Sciences
Tsarigradsko Chaussée 72, 1784 Sofia, Bulgaria*

³*Astronomical Observatory of Kharkiv State University
Sumskaya Street, 310022 Kharkiv, Ukraine*

⁴*Main Astronomical Observatory of Ukrainian National Academy of Sciences
03680, Golosiiv, Kyiv-127, Ukraine*

⁵*International Center for Astronomical, Medical and Ecological Research
03680, Golosiiv, Kyiv-127, Ukraine*

In 1996 the Two-Channel Focal Reducer of the Max-Planck-Institute for Aeronomy has been brought to the Pik Terskol Observatory for use at the 2m-Zeiss-RCC telescope. We describe the instrument and its possibilities. Up to now it has been used for the following solar system projects: astrometry and photometry of the inner satellites of Jupiter, imaging the Io torus with a tunable Fabry-Perot interferometer, photometry and polarimetry of asteroids, imaging photometry and polarimetry of cometary dust and imaging photometry of ions and neutral molecules in comets. These projects are briefly described.

INTRODUCTION

Telescopic studies of solar system objects, in particular of comets, are difficult to schedule at modern astronomical observatories, because of the appearance of such objects frequently is not known sufficiently long in advance to provide sufficient time for a regular proposal of observing time. A contract between the Max-Planck-Institute for Aeronomy (MPAe) and the International Center for Astronomical, Medical and Ecological Research (Center AMER), valid until the end of 2002, allows the MPAe, if needed, access to the 2m-Zeiss-RCC-Telescope at the Pik Terskol Observatory on short notice. The MPAe has brought its Two-Channel Focal Reducer to the Pik Terskol Observatory. This equipment can be made available also to other interested parties. Therefore it seems useful to describe this instrument in some detail and to give an account of the investigations performed up to now under the initiative of the MPAe.

THE TWO-CHANNEL FOCAL REDUCER

The focal reducer principle has first been described by Courtès [4], who also coined the name “réducteur focal”. A focal reducer adapts the imaging elements of the detector to the characteristic size of the object or of the seeing disk. The Two-Channel Focal Reducer of the MPAe was built mainly for observations of cometary plasma but has proven useful for many other tasks [7]. Fig. 1 shows the optical arrangement. Behind the RC (Cassegrain) focus the telescope beam is recollimated by a lens collimator. A color dividing (dichroic) mirror reflects the blue part of the spectrum and transmits the red part. In each “channel” camera lenses form reduced images of the Cassegrain focal plane, which are recorded by two CCD systems. Tab. 1 provides the main parameters of the optical system. The dispersing or polarizing optical elements can be put in the parallel beam either before or after the color divider. Optical elements to be placed in front of the color divider are two tunable and one fixed gap Fabry-Perot etalons and a polarizing beamsplitter. They affect both channels of the instrument. Optical elements put into the parallel beam after color separation are filters, grating prisms, and solid fused silica etalons. A list of available filters is provided in Tab. 2. In order to obtain an unvignetted image on the detector it is necessary that the entrance pupil of the camera lenses should be coincided with the exit pupil of

the collimating system. This condition is difficult to satisfy as the dispersing elements and the color divider, which is needed some space. In order to reduce vignetting to a minimum, if no optical elements are on the telescope side of the color divider, the lower part of the instrument can be moved toward the Cassegrain focal plane in order to minimize the distance between exit pupil of collimator and entrance pupil of the camera lenses at least in this case. An automatized offset guider is available, which can follow moving objects like comets [12].

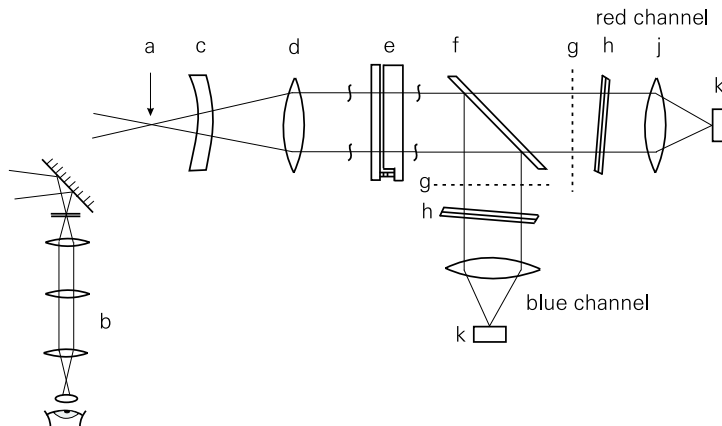


Figure 1: Optical scheme of the Two-Channel Focal Reducer. (a) Cassegrain focal plane, (b) offset guider, (c) field lens, (d) collimator, (e) Fabry-Perot etalon or four-beam Wollaston prism, (f) color divider, (g) Lyot stop (not always present), (h) filter, (j) camera lens, (k) CCD detector. If position (e) is empty, the right part of the instrument can be moved to the left toward Cassegrain focal plane in order to reduce vignetting.

Table 1: Main parameters of the optical system

Collimator	pixel			
	f = 400 mm, exit pupil diameter 50 mm.			
	reflecting	transmitting	reflecting	transmitting
Color dividers	$\lambda < 390$ nm	425 nm < λ	$\lambda < 445$ nm	490 nm < λ
(two dividers per row are listed)	$\lambda < 500$ nm	570 nm < λ	$\lambda < 520$ nm	580 nm < λ
	500 nm < $\lambda < 670$ nm	800 nm < λ	all λ (mirror)	
	blue arm		red arm	
Camera lenses (f=140mm)	355 nm < $\lambda < 510$ nm		420 nm < $\lambda < 700$ nm	
	420 nm < $\lambda < 700$ nm		590 nm < $\lambda < 1000$ nm	
CCDs:	blue sensitive 512×512 pixel		blue sensitive 576×385 pixel	
Pixel size (sky projection)	0.027 mm (1.00 arcsec)		0.022 mm (0.81 arcsec)	
Sky field	7.8×7.8 arcmin		7.8×5.2 arcmin	
Polarimetry field	1.3×1.3 arcmin		1.3×1.3 arcmin	

The instrument has several observing modes. The simplest mode is the mode of *filter imaging*, where broad-band or interference filters are placed into each arm of the focal reducer and the appropriate color divider (see Tab. 1) is selected. Note that it is not possible to use the adjacent UBVRI filters at the same time, one can either use U and V or B and R simultaneously. There is no color divider available, which allows simultaneous imaging in V and I, only B and I can be imaged at the same time.

The device allows a *long slit spectroscopy* with a grating prism (transmission grating cemented on a prism). In this mode a slit is placed at the Cassegrain focal plane. The available grating prism (600 lines/mm) works in the blue arm only. It has a straight-through (center) wavelength of 392 nm and provides a resolution of 0.64 nm in the range of 355–460 nm. Often such a setup is called the faint object spectrograph as it is possible to take an image of the field, identify a faint object, put it on the slit with a telescope offset, insert the slit and take a spectrum. This mode has been used only rarely with the Two-Channel Focal Reducer.

More experience exists with the *interferometry using Fabry-Perot interferometers (FPIs)* [6]. Tab. 3 presents the characteristics of the etalons. The two tunable FPIs provide a single broad fringe covering a large part of the CCD frame and can be looked upon as tunable narrow-band filters with about 3-4 Å FWHM (full width at

Table 2: Filters

Filter name	λ_0^a [nm]	τ_{max}^b	FWHM ^c [nm]	FWTM ^d [nm]	λ_{leak}^e ($\tau > 0.001$) [nm]	τ_{max}^f (leak)	D ^g [mm]	+ additional blocking filter
Wide band filters								
DUG11	338	0.832	75	93			60	
DUG12	338	0.828	75	92			80	
BG24/10	(< 350) - 449	0.936			655 - (> 900)	0.68	80	+ BG39/2
BG24/39	(< 350) - 458	0.753					80	
BG39/2	472	0.928	235				80	
BG39/2	472	0.928	235				60	
B	431	0.946	95	128	636 - 660 754 - (> 900)	0.002 0.79	80	+ BG39/2
Gunn G	519	0.818	65	106			80	
V	531	0.920	102	270			80	
R	680	0.948	111	175			80	
I	797	0.964	153	180			80	
Gunn Z	821 - (> 900)	0.969					80	
HalleUV	390	0.783	103	146			80	
LC660	(< 350) - 665	0.949			774 - (> 900)	0.89	80	
LC661	(< 350) - 669	0.950			775 - (> 900)	0.80	80	
RG66	595 - (> 900)	0.759			(< 350) - 516	0.018	80	
RX	694	0.950	79	101			80	
UG11/4	324	0.824	91	116	691 - 737	0.007	80	
Narrow band filters								
IF358	358.1	0.751	11.4	16.1	673 - (> 900)	0.32	80	+ DUG
IF369	369.3	0.586	9.8	14.0	673 - (> 900)	0.28	80	+ HalleUV
IF390	389.4	0.672	10.5	15.3	655 - (> 900)	0.56	80	+ BG39/2
IF404	403.5	0.678	9.8	13.9	696 - (> 900)	0.017	80	+ BG39/2
IF425	424.2	0.593	6.4	8.9	695 - (> 900)	0.017	80	+ BG39/2
IF426	425.9	0.740	3.7	6.4	521 - 681	0.075	80	+ BB
IF444	443.5	0.808	4.2	6.0	361 - 371 555 - 688	0.003 0.54	80	+ BB
IF501	500.2	0.701	4.1	9.2			80	
IF510	509.4	0.734	4.4	6.4			80	
IF590	589.4	0.591	2.5	3.5			80	
IF614	614.9	0.797	3.2	5.7	734 - 766	0.029	80	+ LC660
IF620	619.5	0.678	3.7	5.9	799 - 801	0.002	80	
IF629	629.1	0.902	2.9	5.2	779 - 787	0.003	80	
IF631	630.8	0.796	3.1	4.4			80	
IF642	641.6	0.580	2.6	3.8			80	
IF658	657.2	0.867	3.2	6.0			80	
IF660	658.5	0.805	28.8	35.4			80	
IF662	662.1	0.881	5.9	8.9			80	
IF667	666.2	0.910	5.5	8.2			80	
IF672	671.9	0.833	3.3	6.1			80	
IF890	876.3 - (> 900)	0.988					80	
IF953	953.7	0.65	1.0		832 - 834	0.004	60 ^h	
IF360	359.7	0.750	3.0	4.1	420 - (> 900)	0.92	60	+ DUG
IF368	367.3	0.773	2.5	3.4	430 - (> 900) 510 - 521	0.92 0.004	60	+ DUG
IF373	373.1	0.395	3.2	6.3	582 - (> 900) 429 - 432	0.86 0.001	60	+ HalleUV
IF407	406.8	0.498	2.3	6.2	672 - (> 900)	0.42	60	+ BG39/2
IF426	425.3	0.683	3.2	5.9	690 - (> 900)	0.85	60	+ BG39/2
IF443	443.2	0.797	4.4	7.9	695 - (> 900) 726 - (> 900)	0.82 0.81	60	+ BG39/2

^a center wavelength^c full width at half of maximum transmission^e range of undesirable transmission ("leak")^g filter diameter^b maximum transmission^d full width at one thousandth of maximum transmission^f maximum of undesirable transmission^h filter fits only into red arm

Table 3: Fabry-Perot-interferometers

Name	kind	useful λ range	reference λ [nm]	free spectral range [nm]	mounted
Queensgate visual	tunable	410-700	627	5.8	before beamsplitter
Queensgate blue	tunable	355-510	374.7	4.3	before beamsplitter
CSIRO visual	fixed airgap	410-700	620	0.21	before beamsplitter
CSIRO red	fused silica	450-700	615	0.26	red arm filter slide
CSIRO blue	fused silica	350-530	400	0.17	blue arm filter slide

half maximum). By proper selection of the interference order one can select wavelength pairs for simultaneous imaging in both arms [7]. The data reduction has been described in [1] and [19]. The fixed-gap FPIs provide fringe systems and can be used for radial velocity measurements. The fused silica ones are tilted with respect to the telescope beam by 4° , in order to avoid internal reflections and to adapt the finesse of the etalons to the spatial resolution of the CCD matrix. The tunable and the fused silica FPIs can be used in tandem.

Of particular interest is the *imaging polarimetry* mode. It is shown in Fig. 2 and has been described in [5]. An assembly of four Wollaston prisms, aligned parallel to each other with an accuracy $< \lambda/4$ is brought in the parallel beam on the telescope side of the color divider in order to let it affect both channels. Two of the four Wollaston prisms are identical pairs, i. e. optically there are only two different Wollaston prisms, one that splits the beam into polarization directions 0° and 90° , and the other into polarization directions $\pm 45^\circ$. In this way the exit pupil of the telescope is split in two halves and four small images with polarization directions 0° , 90° , $+45^\circ$, and -45° are produced on the CCD matrix simultaneously in a single exposure. In rapidly changing objects like comets this simultaneity is the advantage but there are disadvantages: the point spread function of the pair 0° and 90° differs from the pair $+45^\circ$ and -45° . This creates problems if the telescope is not perfectly in focus. The basic limitation, however, comes from the inaccuracy introduced by the flat-fielding process and, ultimately, from the high count rate, which is necessary for imaging polarimetry. Because of the Poisson statistics inherent in the count rate of a CCD, if we want an accuracy of 0.1 % we need 10^6 counts per pixel, which is very hard to achieve on an astronomical object. A similar accuracy is necessary in the flat fields. Experiments show that an accuracy of the degree of polarization significantly better than 1% is very hard to achieve.

In Fig. 1 we mention the Lyot stops, which allow to use the instrument in *the coronagraph mode*. A bright object in the field can be put behind a dark mask or (better) absorbing neutral density glass, located at the Cassegrain focal plane. The Lyot stop is positioned at the location of the exit pupil (image of primary mirror) formed by field lens (c) in Fig. 1 (actually, in our instrument we have two Lyot stops, one in each arm). The Lyot stop covers the rims of both, secondary and primary mirrors and the spider holding the secondary mirror. In this way the diffraction spikes of the bright object behind the mask are significantly reduced. Faint detail close to the bright object may become observable. Presently the coronagraph mode is possible in combination with all other observing modes except of polarization. The Wollaston prism assembly produces 4 different images of the telescope mirror. To cover them all would introduce somewhat larger the light losses.

PROJECTS CONDUCTED AT THE PIK TERSKOL SINCE 1996

Astrometry and photometry of the inner satellites of Jupiter and the Saturnian satellite Phoebe

The coronal skies at the Pik Terskol observatory combined with low atmospheric turbulence provide good conditions for the investigation of faint objects close to bright ones. The observations are conducted with the focal reducer in coronagraph mode. We have been able to observe the inner moons of Jupiter Methis, Amalthea and Thebe and obtained their astrometric positions and brightness as a function of phase angle ([18], [20]). Such observations are most promising in case of Methis, which so far has not been observed at small phase angles.

Io torus

The Io torus is a plasma ring consisting almost exclusively of oxygen and sulphur ions encircling Jupiter at about the distance of the Io satellite. It is created mostly by SO_2 molecules from Io, which are dissociated and ionized by electrons in the Jovian magnetosphere. They radiate in much the same way as in gaseous nebulae. The work conducted at the Pik Terskol is an extension of [19]. One of the aims is to support measurements of the Galileo and Cassini space probes in 2000. Using the coronagraph setup and the visual tunable Fabry-Perot interferometer we observe the red [SII] doublet at 6716.4 and 6730.9 Å and the lines of [SIII] at 9530.9 and

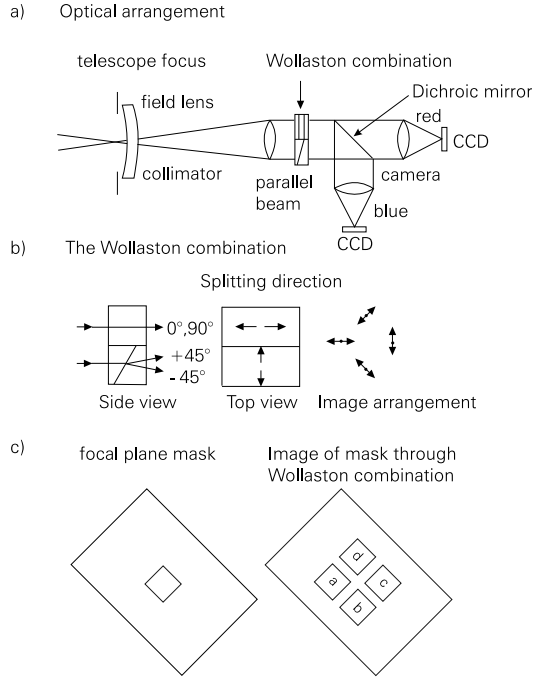


Figure 2: Optical scheme of the Two-Channel Focal Reducer in polarimetric mode.

6312.1 Å. The lines of [SIII] show the hotter material and the line ratio allows to derive the electron temperature while the [SII] lines show the cooler material and the line ratio provides electron density. Morphological details observed under excellent seeing conditions indicate a warping of the torus.

Asteroid polarimetry and photometry

Asteroid regolith has optical properties surprisingly similar to cometary dust. Since 1996 two programs concerning the asteroids have been conducted, namely the polarimetric observations of 2100 Ra-Shalom asteroid at large phase angle ([13], [14]), and photometric and polarimetric observations of 64 Angelina asteroid near opposition [23].

Cometary dust

Since 1996 we have observed C/1995 O1 Hale-Bopp, C/1996 Q1 Tabur, 46P/Wirtanen, 21P/Giacobini-Zinner, C/1998 U5 (Linear), C/1999 H1 (Lee), C/1999 J3 (Linear), and C/1999 S4 (Linear) comets. Most of these comets were observed through the blue and red continuum filters at 443 nm and 642 nm. The passbands of these filters are considered free from emissions of cometary molecules or ions and show only the solar light, scattered by the cometary dust particles. If possible, the imaging polarimetry has been also done in these passbands. Some comets, in particular the larger ones like Hale-Bopp comet, show a structured dust coma with “jets” and “shells”, which are visible in the polarization and color images as well. In [10] it is concluded that the jet particles have optical properties like submicron grains but experience a radiation pressure similar to larger grains. It is pointed to the aggregate nature of the jet particles (see also [21], [22]). Another important result is the negative wavelength gradient of polarization found in comet 21P/Giacobini-Zinner, which distinguishes this comet from almost all other comets ([15], [16]).

Cometary gas and plasma

We have observed cometary gas and plasma in all comets mentioned in the previous paragraphs, except C/1999 H1 Lee. The work includes derivation of the water production rate from observations of the [OI] 6300 Å line with Fabry-Perot etalon CSIRO red (Tab. 3), using the radial velocity of the comet to separate the cometary emission from terrestrial airglow [11]. The water production rate was also derived from observations of H₂O⁺ ([24], [8], [11]). Comet 46P/Wirtanen, the target of the ESA Rosetta mission, was observed as well and a water production rate has been determined ([9], [24]). The cosmochemically important ratio of H₂O⁺/CO⁺ has been derived in [3] and [8] for several comets. Plasma velocities have been published in [2] and [3]. CN and NH₂ maps of comet C/1999 J3 (Linear) have been analyzed in [17]. For more details we refer the reader to two other contributions to this conference, [11] and [17].

REFERENCES

- [1] *Bonev T., Jockers K.*, H_2O^+ ions in the inner plasma tail of comet Austin-1990-V // *Icarus*–1994.–**107**, 335–357.
- [2] *Bonev T., Jockers K., Credner T.*, Comet Hale-Bopp: velocity field of ions from Fabry-Prot imaging // *Earth, Moon and Planets*–1997.–**77**, 245–252.
- [3] *Bonev T., Jockers K., Korsun P., Karpov N., Sergeev A.*, H_2O^+ and CO^+ in comet C/1999 J3 (Linear) // *Bulgarian Journal of Physics*–2000.–, submitted.
- [4] *Courtès, G.*, Méthodes d'observation et étude de l'hydrogène interstellaire en émission // *Ann. d'Astrophys.*–1960.–**23** N 2., 115–217.
- [5] *Geyer E. H., Jockers K., Kiselev N. N., Chernova G. P.*, A novel quadruple beam imaging polarimeter and its application to Comet Tanaka-Machholz 1992 X // *Astrophys. Space Sci.*–1996.–**239**, 259–274.
- [6] *Jockers K.*, Astronomical observations of comets and the Io torus using Fabry-Perot-Interferometry, in: *Tridimensional Optical Spectroscopic Methods in Astrophysics*, IAU Colloquium 149, (edited by G. Comte and M. Marcelin), A. S. P. Conf. Ser.–1995.–Vol. **71** pp. 182–187, Astron. Soc. Pacific, San Francisco.
- [7] *Jockers K.*, A two-channel focal reducer for small (diameter ≥ 1 m) telescopes // *Exper. Astron.*–1997.–**7**, 305–318.
- [8] *Jockers K., Bonev T., Credner T.*, Observations of ions in comets: A contribution towards understanding the comet-solar wind interaction // *Astrophys. Space Sci.*–1999.–**264**, 227–234.
- [9] *Jockers K., Credner T., Bonev T.*, Water ions, dust and CN in comet 46P/Wirtanen // *Astron. Astrophys.*–1998.–**335**, L56–L59.
- [10] *Jockers K., Rosenbush V. K., Bonev T., Credner T.*, Images of polarization and colour in the inner coma of comet Hale-Bopp, *Earth, Moon and Planets*–1997.–**78**, 373–379.
- [11] *Jockers K., Bonev T., Korsun P., Karpov N., Sergeev A., Tarady V.*, Water production of comets derived from observations of [OI] (6300 Å) and H_2O^+ (6150 Å): Comets C/1998 U5 (Linear) and C/1999 J3 (Linear) // this issue.
- [12] *Karpov N. V., Jockers K.*, Information support of observations at the 2-m telescope of Pik Terskol observatory // *Kinematika i fizika nebesnykh tel*–2000.–**16/4**, in print.
- [13] *Kiselev N. N., Rosenbush V. K., Jockers K.*, Polarimetry of asteroid 2100 Ra-Shalom. A comparison of polarization-phase dependences for C- and S-type asteroids and comets // *Astron. Vestnik*–1999.–**33**, 222–230.
- [14] *Kiselev N. N., Rosenbush V. K., Jockers K.*, Polarimetry of asteroid 2100 Ra-Shalom at large phase angle // *Icarus*–1999.–**140**, 464–466.
- [15] *Kiselev N. N., Jockers K., Rosenbush V. K., Velichko F. P., Bonev T., Karpov N.*, Anomalous wavelength dependence of polarization of comet 21P/Giacobini-Zinner // *Planet. Space Sci.*–2000.–**48**, 1005–1009.
- [16] *Kiselev N., Jockers K., Rosenbush V. K.*, Organic matter in dust particles of Comet 21P/ Giacobini-Zinner and the Draconid meteoroids // this issue.
- [17] *Korsun, P. P., Jockers, K.*, CN and NH_2 atmospheres of Comet/1999 J3 (Linear) // this issue.
- [18] *Kulyk I., Jockers K., Karpov N., Sergeev A.*, Near-infrared photometric observations of the inner Jovian satellites // this issue.
- [19] *Küppers M., Jockers K.*, A multi-emission study of the Io plasma torus // *Icarus*–1997.–**129**, 48–71.
- [20] *Ledovskaya I., Jockers K., Karpov N., Sergeev A.*, Astrometric CCD observations of Jovian inner satellites Thebe, Amalthea, and Saturnian satellite Phoebe in the 1998 opposition // *Kinematika i fizika nebesnykh tel*–1999.–**15/6**, 483–485.
- [21] *Petrova E. V., Jockers, K. Kiselev, N. N.*, Rasseyanie sveta aggregatnymi chastitsami, soizmerimymi s dlinoj volny: prilozhenie k kometnoj pyli // *Astron. Vestnik*–2000.–, in press.
- [22] *Petrova E. V., Jockers, K. Kiselev, N. N.*, Light scattering by aggregates with sizes comparable to the wavelength: an application to cometary dust // *Icarus*–2000.–, in press.
- [23] *Rosenbush V. K., Kiselev N. N., Jockers K., Korokhin V. V., Shakhovskoy N. M., Efimov Yu. S.*, Optical polarimetry of the Galilean satellites, Iapetus, and 64 Angelina near opposition // this issue.
- [24] *Wegmann R., Jockers K., Bonev T.*, H_2O^+ ions in comets: models and observations, *Planet. Space Sci.*–1999.–**47**, 745–763.